Theses and Dissertations

2008

Mechanisms and developments of magnetic source MRI

Yiqun Xue
University of Iowa

Recommended Citation

MECHANISMS AND DEVELOPMENTS OF MAGNETIC SOURCE MRI

by

Yiqun Xue

An Abstract

Of a thesis submitted in partial fulfillment
of the requirements for the Doctor of
Philosophy degree in Biomedical Engineering
in the Graduate College of
The University of Iowa

December 2008

Thesis Supervisor: Associate Professor Jinhu Xiong

ABSTRACT

Magnetic source MRI (msMRI) has been developed recently for direct detections of neuronal magnetic fields to map brain activity. However, whether MRI can be used for direct detection of neuronal activity is a matter of debate. Controversial theoretical and experimental results have been reported. In this work, theoretical modeling and experimental validation have been presented to demonstrate that the neuronal current signal is in the detectable range and could be detected by MRI. In the theoretical modeling section, we present an improved current-dipole model to compute magnetic field generated by neural firing and to calculate MRI signal changes resulting from the neuronal magnetic field. Neuronal magnetic field were estimated based on a synchronized activity of multiple neurons. Our results show that neuronal magnetic field can potentially generate up to a few percent changes in MRI magnitude signals. Phases of MRI signal tend to be destructively added and are insensitive to neuronal magnetic field in the activated region when the distribution of the activated dendrites is symmetrical. Our modeling implies that direct MRI detection of neuronal activity is possible. In the experimental validation section, a rapid median nerve stimulation paradigm has been used to detect the neuronal activity. The experiments were performed on six normal human participants to investigate the temporal specificity of the effect, as well as inter- and intra-subject reproducibility. Significant activation of contra-lateral primary sensory cortex (S1) was detected 80ms after stimulation onset (corresponding to the P80 evoked potential peak). The 80 ms latency S1 activation was observed over 3 independent sessions for one subject and for all 6 participants. The magnitude of the signal change was 0.2% - 0.3%. Coinciding with our expectations, no S1 activation was

found when MRI data acquisitions were targeted at the N20 and P30 peaks because of mutual cancellation of magnetic fields generated by those peaks. The results demonstrated good reproducibility of S1 activations and indicated that the S1 activations most likely originated from neuronal magnetic field rather than hemodynamic response.

Abstract Approved: _____
                                                  Thesis Supervisor

                                                  _____
                                                  Title and Department

                                                  _____
                                                  Date

MECHANISMS AND DEVELOPMENTS OF MAGNETIC SOURCE MRI

by

Yiqun Xue

A thesis submitted in partial fulfillment
of the requirements for the Doctor of
Philosophy degree in Biomedical Engineering
in the Graduate College of
The University of Iowa

December 2008

Thesis Supervisor: Associate Professor Jinhu Xiong

Graduate College
The University of Iowa
Iowa City, Iowa

CERTIFICATE OF APPROVAL

_____

PH.D. THESIS

_____

This is to certify that the Ph.D. thesis of

Yiqun Xue

has been approved by the Examining Committee
for the thesis requirement for the Doctor of Philosophy
degree in Biomedical Engineering at the December 2008 graduation.

Thesis Committee: _____
                             Jinhu Xiong, Thesis Supervisor

                     _____
                             Edwin L. Dove

                     _____
                             Thomas J. Grabowski

                     _____
                             Vincent A. Magnotta

                     _____
                             Joseph M. Reinhardt

                     _____
                             Daniel R. Thedens

ACKNOWLEDGMENTS

This dissertation could not be completed without contributions from a number of people. I would like to make a grateful acknowledgement to them.

I would first like to thank my advisor Dr. Jinhu Xiong for his invaluable guidance which will help me throughout my professional career. I would like to thank Dr. Vincent Magnotta for his help in MR data acquisition. I would like to thank Dr. Thomas Grabowski for his expertise in neuroscience. I would like to thank Dr. Peter Seaba for his technical assistance. I would also thank all other committee for their help.

TABLE OF CONTENTS

LIST OF TABLES

LIST OF FIGURES

CHAPTER I

INTRODUCTION

Since its development in the early 1990s (Belliveau 1991; Bandettini 1992; Kwong 1992; Ogawa 1992), functional magnetic resonance imaging (fMRI) has been widely used to study the functional organization of the human brain. Current fMRI techniques rely on measuring regional cerebral hemodynamics (i.e., blood flow and blood oxygenation) to infer information about neuronal activity. While having greatly enhanced our understanding of the functional organization of the human brain, these indirect measurements bear several limitations. Because coupling between neuronal activity and regional cerebral hemodynamics is complex and non-linear, changes in regional cerebral hemodynamics may not accurately reflect underlying neuronal activity. Both temporal and spatial information of current fMRI are degraded and distorted. A novel fMRI technique which is called magnetic source MRI (msMRI) (Xiong 2003b) has been developed recently for directly assessing neuronal function.   The technique is based on directly detecting MRI signal changes in response to the changes in magnetic fields induced by neuronal firing and offers improved spatial localization and temporal resolution.

CHAPTER II

BACKGROUND

Current Brain Mapping Techniques

Approaches for studying human brain function have developed promptly over the past 20 years. Nevertheless, current brain mapping techniques, such as positron emission tomography (PET), functional magnetic resonance image (fMRI), event-related potential (ERP), and magnetoencephalography (MEG), generally represent a trade-off between a excellent spatial resolution and temporal resolution.

Current fMRI Technique

First reported in 1991 (Belliveau et al., 1991), fMRI has become a highly productive and rapidly growing field over the past decade. Currently used fMRI techniques, however, depend on measuring regional cerebral hemodynamics (blood flow and blood oxygenation) to infer neural activation, rather than detecting neuronal activity directly. Because the coupling between regional cerebral hemodynamics and neuronal activity is complex and non-linear, this indirect measurement has several limitations. First, regional cerebral hemodynamics does not necessarily always reflect neuronal activity. Regional cerebral hemodynamics could change (for example, drug effects) without underlying neuronal activity change. Second, BOLD contrast is vascular origin. Large draining veins can dominate regions of the image. Hence, BOLD contrast may not always be a reliable indication of the area of neuronal firing (Lai et al., 1993). Third, the cerebral hemodynamics responses are much slower (in the order of a second) than neuronal firing (in the order of a millisecond). Temporal resolution of the hemodynamic measurement is, therefore, limited and downgraded with respect to the

underlying neural activation.

Current MEG and ERP Techniques

Magnetoencephalography (MEG) and electroencephalography (EEG) are based on the detection of electromagnetic signal produced by neuronal populations. Although both of MEG and ERP can offer superior temporal resolution (in the order of a millisecond), their spatial resolutions are typically poor. Relying on information detected at the scalp to localize active sites inside the brain, both EEG and MEG require solving an inverse problem, which leads to spatial uncertainty in the localization of electromagnetic sources. Another limitation for ERP and MEG is that both techniques are good for detecting the signal from the brain surface but unable to detect neuronal activities deep in the brain.

msMRI Technique.

Mapping neuronal activity with MRI by detecting neuronal magnetic fields is theoretically straightforward. Neuronal activity generates ionic current along the axon and dendrites. This neuronal current will generate a weak, transient magnetic field around neuron. The component of this neuronal magnetic field parallel to the B_0 field of MRI scanner will change the precession rate of nuclear spins. Spins exposed to the neuronal magnetic field will lose phase coherence and result in a decrease in MRI signal strength. It is well established by MEG that magnetic fields generated by cortical neuronal activity are detectable even at the scalp ($\sim 10^{-13}$ T (Cohen 1968)). The magnetic field at the source (the cerebral cortex) will necessarily be much stronger than at the scalp (2 - 4 cm away), but it remains to be proven that the msMRI effect is strong enough to be detectable and useful.

The feasibility of directly mapping neuronal activity has been addressed theoretically.

Divergent conclusions were reached by investigators considering different dipole models or measuring different parameters (i.e. phase and magnitude imaging). Initially, Singh (1994) used an electrical current phantom to investigate the possibility of detecting the evoked neuromagnetic field. The neuronal magnetic field inside the brain was calculated on the basis of the field observed on the surface of the skull. It was reported that the required measurement of phase shifts was twenty-fold smaller than the sensitivity of the scanner they used. However, it is possible that the local neuronal magnetic field is much larger than they predicted since opposite neuronal currents have a cancellation effect which results in a much smaller field on the skull. Konn (2003) modeled neuronal current flow as an extended current dipole located in a conducting sphere. They demonstrated that the minimum detectable dipole strength by nuclear magnetic resonance under normal experimental conditions was similar in magnitude to dipole strengths from evoked neuronal activity. Further, it has been reported by Bodurka (2002) and Konn (2003) that phase imaging is a better approach than magnitude imaging based on the extended current dipole model. Xue (2006) presented a theoretical model which modeled each dendrite as a finite size dipole and considered contributions from all dendrites located in a typical MRI voxel. They concluded that the magnitude change of MRI signal is much more significant than phase change of the signal on a voxel scale, theoretically reaching magnitudes of as much as 2%. Pell (2006) further optimized MR sensitivity to transient and weak currents and suggested that it should be possible to detect current in nerves using magnitude imaging. Blagoev (2007) and Cassara (2008) presented more realistic models to simulate neuronal activities of single and multiple neurons. Both of them modeled the spatiotemporal distributions of the neuronal magnetic field. They

concluded that MR signal changes were in the detectable range but depend highly on neuronal morphology and physiology properties.

Experimental results have also been reported by several labs. Early phantom tests (Scott 1992; Bodurka 1999; Bodurka 2002) showed that it is possible to detect the magnetic fields of the order of 10^{-10} T, which is similar to the magnitude of the magnetic field induced by neuron firing (Romani 1989; Wikswo, 1989). The feasibility of direct detection of neuronal magnetic field has also been explored in human subject experiments. Kamei (1999) initially applied this technique to obtain maps of human brain activity by using motor and sensory stimulation paradigms. It was suggested that neuronal current induced MRI signal changes are dependent on the polarity of field gradient but other causes (i.e. susceptibility effect) are not, and that neuronal current effects could therefore be acquired by subtracting functional images acquired with opposite field gradients. Song (2001), Truong (2006) demonstrated that a small neuronal current could be directly detected using MRI by measuring small spatial displacements induced by the Lorentz force on the conducting materials. In 2003, Xiong (2003a) reported that neuronal activity in a visuomotor paradigm could be detected using gradient echo (GE) EPI sequence with a high temporal resolution (100 ms). Bianciardi (2004) subsequently presented preliminary results showing detection of a neuronal magnetic field effect using a spin echo (SE) MRI sequence. Liston (2004) reported a successful MRI detection of activations associated with generalized spike-wave discharges in a patient with epilepsy. Chow (2006a, b) directly detected spectral components of the magnetic fields of ionic currents caused by firing of optic nerve axons in response to visual strobe stimulation and reported a higher detectability for magnitude imaging than

phase imaging. Petridou (2006) used organotypic rat-brain cultures *in vitro* and demonstrated that spontaneous neuronal activity could be detected directly using MRI in the absence of a cerebrovascular system. Several negative results have also been published. A notable result was reported by Chu (2004), who used a clever embedded binary m-sequence probe method to detect the neuron activity in visual cortex. They reported the absence of any rapid phase or magnitude changes in this experiment. Similarly, Parkes (2007) presented a visual stimulation paradigm with random intervals to minimize the prediction effects. Their results showed no activity that could be attributed to the neuromagnetic signals. Tang (2008) reported failure to detect the signal changes which was temporally correlated with the timings of evoked response potentials by using a hybrid ms/BOLD event related design.

<div align="center">Significance and Advantages of msMRI</div>

The msMRI technique offers several advantages over current neuroimaging methods. It appears to provide better combined spatio-temporal resolution than any currently used non-invasive neuroimaging methods. Compared with "traditional" fMRI and PET, msMRI offers much higher temporal resolution, with no loss of spatial resolution. Detecting brain activity via the cerebral hemodynamic and metabolic responses to neural firing, the temporal resolutions of fMRI and PET are ultimately limited by the slow response function of cerebral hemodynamics, which is on the order of seconds. Furthermore, their inferences regarding neuronal activity are necessarily complicated by the variability of coupling between neuronal activity, cerebral hemodynamics, and metabolism (Fox 1986). Compared with ERP and MEG (Cohen 1968; Lewine 1995), msMRI offers higher spatial accuracy. The msMRI effects are spatially mapped in the

same manner as traditional MRI techniques and involve no inverse problem.   In addition, ERP and MEG are each limited in the activation geometries they can detect and are unable to detect neuronal activities deep in the brain; msMRI has no such limitation. Therefore, successful development of msMRI technique will provide a powerful tool for mapping human brain functional organizations.

CHAPTER III

THEORY AND METHODS

Theoretical Modeling

Single Neuron Model

A neuron in the brain typically consists of a single axon and multiple dendrites. We model each dendrite or axon using intracellular current i_i and extracellular current i_e (Figure 1a). Such a combination of source and sink of equal magnitude is called a current dipole. For convenience, we define that the y-axis is along the B_0 field and the z-axis is along the dendritic current.

For any observation point P outside a neuron (Figure 1b), magnetic field can be calculated according to Biot-Savart law:

$$B = \int \frac{\mu_0 i}{4\pi} \frac{dz \times \mathrm{r}}{r^3} \qquad (1)$$

where **B** is the neuronal magnetic field, μ_0 is magnetic permeability of space, i is neuronal currents which include internal, external and through-membrane current, dz is line element along the current, vector **r** is the distance from the current element to the observation point.

This equation is suitable to both dendrites and axons. However, for myelinated axons, the majority of neural current concentrates at nodes of Ranvier and is through-membrane current. It can be easily demonstrated that the through-membrane current generates no net magnetic field outside the neuronal membrane and can be ignored (Swinney 1980). Therefore, contributions of a myelinated axon to overall magnetic field are small and can

thus be ignored. As the majority of axons in the brain are myelinated, dendrites are the main source of neuronal magnetic field.

Theoretically, both intracellular current i_i and extracellular current i_e will contribute to the neuronal magnetic field. It, however, has been shown that the contribution from the extracellular current is two orders of magnitude smaller than that from intracellular current (Okada 1997; Swinney 1980). Effects of the extracellular current, therefore, can be safely ignored (Okada 1997; Swinney 1980).

Since the length of a dendrite is much longer than the radius, the magnetic field generated by current dipole at any observation point inside the dendrite can be conveniently calculated according to Ampere's circuital law. Considering the cylindrical symmetry of a dendrite and assuming a uniform current density, the magnitude of the field is related to the intracellular current, i_i, by:

$$B = \mu_0 \frac{d}{2\pi a^2} i_i \tag{2}$$

where d is the radial distance from the observation point to the dendrite, a is radius of dendrite. The neuronal magnetic field at any observation point can be calculated using equations 1 and 2.

While all our calculations are based on Equations 1 and 2, it is worthwhile to discuss some extreme cases. When the observation point is close to the dendrite, $d \ll l$, where l is the length of dendrite, Equation 1 can be simplified as:

$$B = \frac{\mu_0 i_i}{2\pi d} \tag{3}$$

This is the equation to calculate magnetic field around an infinite long wire. That is, our modified current dipole model can be approximated by an infinite long wire model when the observation point is very close to the dendrite.

When the observation point is far away from the dendrite, $d \gg l$, Equation 1 can be simplified as:

$$B = \frac{\mu_0 i_i l}{4\pi d^2} \tag{4}$$

This is the current dipole model commonly used in MEG for computing magnetic fields generated by neural firing. In other words, our modified current dipole model agrees well with the commonly used current dipole model when the observation point is far away from the dendrite.

Effects of Neuronal Magnetic Field on MRI Signals

The component of neuronal magnetic field, B_n, parallel to the B_0 (of the MRI scanner) will cause the spins at point (x, y, z) in the transverse plane to acquire additional phases, $\varphi_1(x, y, z)$, which depend on strengths of the local neuronal magnetic field, $B_n(x, y, z, t)$.

$$\varphi_1(x, y, z) = \int_0^{TE} \gamma B_{n//}(x, y, z, t)dt = \int_0^{TE} \gamma B_n(x, y, z, t)\cos(\theta)dt \tag{5}$$

where *TE* represents the echo-time, θ is the angle between B_0 and B_n, γ represents the gyromagnetic ratio, and $B_{n//}$ is the component of B_n parallel to the B_0. The majority of $B_{n\perp}$, which is the component of B_n perpendicular to the B_0, will have no net effect on the spins. Only a small fraction of $B_{n\perp}$ at the Larmor frequency will act like a B_1 field to rotate the spins at a point (x, y, z) away from the x-y plane. The fraction is typically very small. The effect of $B_{n\perp}$, therefore, can be ignored.

The MRI signal observed at a point (*x, y, z*) after 90^0 radio-frequency excitation is

related to phase changes induced by the neuronal magnetic field by:

$$s(x, y, z) \propto \rho(x, y, z)e^{i\varphi_1(x,y,z)} \tag{6}$$

where $\rho(x, y, z)$ is spin density, and $\varphi_1(x, y, z)$ is defined by equation 5. The MRI signal

for an image voxel is an integral of $s(x, y, z)$ over the voxel:

$$S \propto \int_0^{\Delta x} \int_0^{\Delta y} \int_0^{\Delta z} \rho(x, y, z)e^{i\varphi_1(x,y,z)}dxdydz \tag{7}$$

where Δx, Δy, and Δz are the dimensions of the voxel, $\rho(x, y, z)$ is spin density. The

magnitude of MRI signal is vector sum of all spins in the voxel. Since the additional

phase can be positive or negative, the vector in the direction which is perpendicular to the

rotating frame of reference will cancel out each other and can be ignored. The magnitude

of MRI signal in the rotating frame of reference, therefore, is decreased by a factor of

$\cos(\varphi_1(x, y, z))$ and the magnitude change can be written as:

$$\Delta S_m = \int_0^{\Delta x} \int_0^{\Delta y} \int_0^{\Delta z} \rho(x, y, z)(1 - \cos(\varphi_1(x, y, z)))dxdydz \tag{8}$$

Since the additional phase shift $\varphi_1(x, y, z)$ is pretty small and very close to 0, according to

the Taylor expansion, equation 8 can be rewritten as

$$\Delta S_m \approx \int_0^{\Delta x} \int_0^{\Delta y} \int_0^{\Delta z} \rho(x, y, z)\frac{\varphi_1(x, y, z)^2}{2}dxdydz \tag{9}$$

The magnitude change of MRI signal is roughly relative to the square of phase shift

induced by neuronal magnetic field. This is consistent with the simulation results

reported by Xue (2006).

Optimal TE

For BOLD fMRI, the signal percentage change is linear related to TE and the

contrast to noise ratio (CNR) is known to be optimized when TE=T2*. However, msMRI

measures the accumulated dephasing effects of neuronal activity during the entire TE, msMRI signal should be stronger if a longer TE is used. Assuming these fired neurons are uniformly distributed within TE, the additional phase shift induced by neuronal magnetic field is linear with the length of TE. Based on equation (9), this relationship leads to

$$\Delta S_m \propto TE^2 \qquad\qquad (10)$$

By taking account into the effect of T2* decay of spins and assuming noise is constant, the contrast to noise ratio (CNR) is related to

$$CNR \propto TE^2 \cdot e^{-\frac{TE}{T_2^*}} \qquad\qquad (11)$$

It can be concluded that the maximal CNR happens when TE equals twice T2*. The T2* value varies with brain area and also highly depends on shimming. For grey matter, which is the tissue compartment we are interested in, the commonly used T2* for gray matter at 3T scanner is 40ms (Norris 2003). The optimized TE is 80ms. When the activated neurons are not uniformly distributed in TE (i.e. normal distribution) or with limited duration, the optimal TE is less than twice T2*.

Experimental Validation

We used a rapid median nerve stimulation paradigm to validate the feasibility of msMRI technique. Unilateral stimulation of median nerve activates the contralateral primary somatosensory cortex (SI). A series of somatosensory evoked potentials (SEPs) (i.e. N20-P30-N45-P80) in area SI have been reported by Allison (1989a, b) who directly recorded SEPs from the exposed cortical surface. The timing information, therefore, directly reflects the neuron activity in the cortex (Allison 1989a, b). The earliest cortical response peaks at 20ms after median nerve stimulation. This negative peak (N20) originates at area 3b of the SI cortex. In other words, the direction of the intracellular

current is from the deep towards the superficial layers of area 3b of the SI cortex, consistent with excitation in the deep cortical layers. The next deflection has the opposite polarity and peaks at 30-35 ms (P30) after stimulation. This P30 response most probably reflects net intracellular current from surface to depth in the SI cortex. The late potential, P80, was reported by Allison (1989b) and this component localizes to Brodmann area 2 (BA2).

Subjects

Six healthy subjects (two men and four women, aged 25-32) participated in this study. All subjects were right handed. Informed consent in accordance with local and federal standards was obtained from each participant prior to the study. Subjects lay supine inside the magnet bore throughout the experiment during the presentation of electrical stimuli. Head movement was minimized by mild restraint and cushioning.

Paradigm

Unilateral stimulations were delivered to the median nerve at the right wrist by a Grass S8 stimulator. The electrical noise from the stimulator is not significant based on our phantom and human test. The electric stimulus was a square wave pulse with a duration of 0.2 msec. The shock intensity was adjusted to obtain a thumb twitch. Pulse amplitudes ranged from 80-120 V. Subjects were asked not to actively perform any task, but to keep still and awake. By only detecting the passive neuron response to the electrical stimulation, variances in response timing due to subject motivation and attention have been minimized. Because msMRI directly detects neuronal response and has high temporal resolution, reducing uncertainties in stimulus timing can greatly enhance the sensitivity for msMRI signals that occur in a narrow temporal window.

Unilateral stimulation of median nerve activates the contralateral primary somatosensory cortex (SI). A series of somatosensory evoked potentials (SEPs) (i.e. N20-P30-N45-P80) in area SI have been reported by Allison (1989a, b) who directly recorded SEPs from the exposed cortical surface. The timing information, therefore, directly reflects the neuron activity in the cortex (Allison 1989a, b) To investigate temporal properties of msMRI signals, we targeted our data acquisitions at different components of the SEPs (N20/P30 and P80). The earliest cortical response peaks at 20ms after median nerve stimulation. This negative peak (N20) originates at area 3b of the SI cortex. In other words, the direction of the intracellular current is from the deep layer towards the superficial layer of area 3b of the SI cortex, consistent with excitation in the deep cortical layers. The next deflection has the opposite polarity and peaks at 30-35 ms (P30) after stimulation. This P30 response most probably reflects net intracellular current from surface to depth in the SI cortex. The late potential, P80, was reported by Allison (1989a) and this component localizes to Brodmann area 2 (BA2).

There are several advantages for the rapid median nerve stimulation design over previous designs. The stimulus onset asynchrony (SOA) and timing of the neuronal response could be accurately controlled. Moreover, the BOLD effect was minimized by the design. Different SOAs were used to detect the different response components and demonstrate the temporal specificity of msMRI effects.

Protocol and Data Acquisitions

All MRI data were acquired at Siemens 3.0 T Trio scanner (Siemens Medical Solutions, Erlangen, Germany). T1-weighted anatomical images were acquired to facilitate the precise determination of the brain structures. The parameters for

T1-weighted images were: TR=1590 ms, TE=2.48 ms, flip angle=10 degrees, voxel size=0.86 x 0.86 x 6 mm^3. Both BOLD imaging and msMRI imaging were performed on each subject. BOLD imaging was performed first to identify activated brain regions. Sixteen slices were selected and a conventional block design was used with three 40 sec off-on cycles. The stimuli were delivered every two seconds during the task block. A gradient echo EPI pulse sequence was used with imaging parameters: TR=2000 ms, TE=40 ms, flip angle=80 degree, in-plane resolution 3x3 mm^2 and slice thickness 5 mm with 1 mm gap. Activation maps were calculated immediately after the scan by using an online t-test analysis.

In the msMRI phase of the experiment, a gradient echo EPI pulse sequence was used with TR/TE/flip angle parameters of 300 ms/60 ms/40 degree. An inter-stimulus-interval (ISI) of 600 ms was used to drive the BOLD MRI signal to steady state. Each run included 600 stimulation ON/OFF cycles with two images for each cycle (one ISI). Stimulus delivery was synchronized with the trigger signal from MRI scanner to provide accurate control on timing. Three contiguous slices were scanned with ascending order. The middle slice was targeted on the subjects' S1 area. In this experiment, we were concerned to detect the dephasing effect of neuronal magnetic field in this area. Three different SOAs were used in our msMRI experiments. Figure 2a shows the timing for detecting msMRI activation at 80ms latency. Data was acquired from 50 ms to 110 ms after stimulation onset so that the 80 ms latency component completely fell into TE. Figure 2b shows the timing for detecting the early components (0~60 ms). In Figure 2c, the electrical stimuli (100 ms after the trigger from scanner) were delivered after the target slice was scanned. For this case, the data from the target slice should not contain

any neuronal current effects induced by stimulation. Control scans in which no stimulation was applied were also performed for every subject.

Data Analysis

The MRI images were processed in the MATLAB environment (MathWorks Inc., Natick, MA, USA). The first 40 images of each run were discarded to allow hemodynamics and MRI signal to reach a steady state. A two-dimensional (2-D) motion correction was carried out to minimize in-plane motion. Data interpolation between image slices was purposely avoided because different slices were acquired at different times. Voxel-by-voxel linear detrending was used to remove the linear drift of the MRI signal. The heartbeat rate and respiration rate of the subject were measured before each scan and a proper temporal high pass filter was then applied to remove the respiration frequency and the aliased frequency of the heartbeat. A mean image was created for each off-on cycle by averaging the time-series in the cycle, and then subtracted from each image to create residual images. A 2-D spatial Gaussian filter with a full width at half magnitude (FWHM) of 4.5 mm was applied. A group student's t-test was then performed on the residual images. The t map was then thresholded using an intensity threshold of 3.0 (P< 0.0013) and cluster size threshold of two voxels to detect significant activation assuming the msMRI activation extended several mm^2.
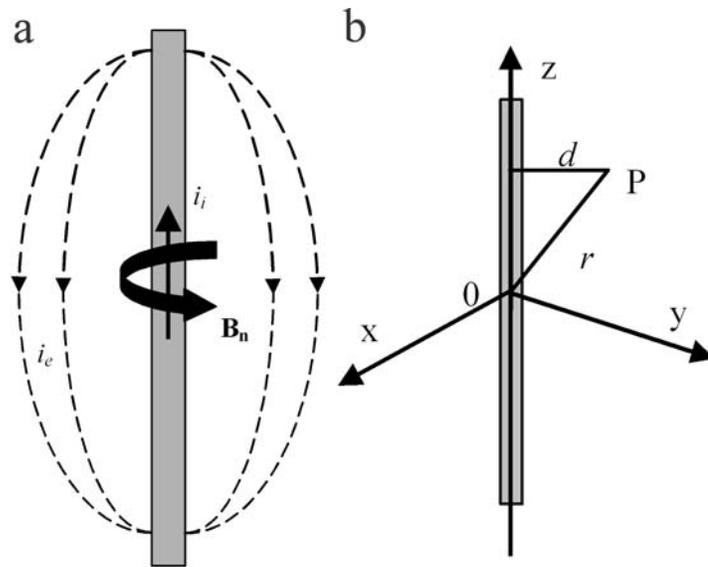
Figure 1. Current dipole model commonly used for a dendrite and/or axon. The current flows along the dendrite and axon, and flows out into the external medium from one end and back at another end. The Biot-Savart law is used to calculate the magnetic field at point P. Dendritic current is along the z-axis and B_0 is along the y-axis.
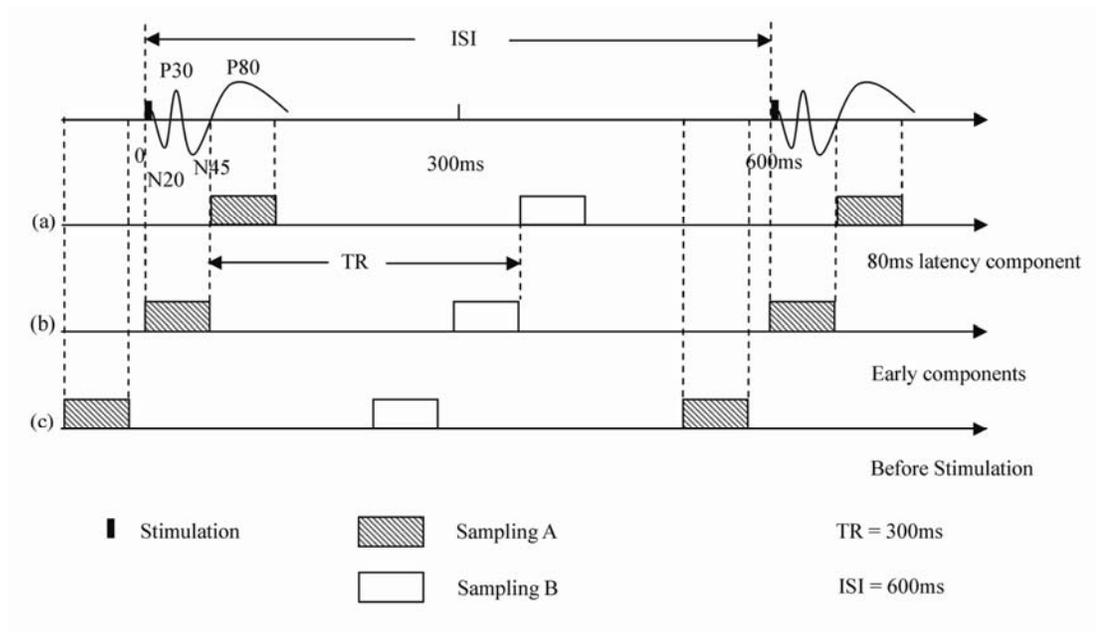
Figure 2. Fast median nerve stimulation paradigm

(a) The msMRI paradigm for detecting the 80 ms latency component. Data were acquired 50ms~110ms after stimulation onset (sampling A).

(b) The msMRI paradigm for detecting the early components. Data were acquired 0ms~60ms after stimulation onset (sampling A).

(c) Data were acquired (-100~-40ms), i.e., before stimuli were presented (sampling A). No msMRI effects were obtained in this scan. Sampling B is control image.

CHAPTER IV

RESULTS

Theoretical Modeling

Base on our modified dipole model discussed in theory section, we first estimate the distribution of neuronal magnetic field. We start from a simple one-dipole model; and then a two-dipole system and more realistic multi-dipole system are modeled. Interactions of spins and neuronal magnetic field are considered.   Both magnitude MRI signal changes and phase MRI signal changes are calculated.

Distribution of Neuronal Magnetic Field

One-dipole System

The magnetic field generated by a single dendrite is shown in Figure 3. Here, B_0 is along the y-axis and dendritic current is along the z-axis. Figure 3 shows that the magnitude of magnetic field linearly increases as the radial distance increases, peaks on the surface of the dendrite, and then quickly declines.   This field is concentrated in and around the dendrites.

Two-dipole System

In a two-dipole system, we take into account the effect of the spatial relationship between dendrites (current dipoles) and magnetic field distributions.   Figure 4a & 4b show a two-dipole system with parallel (two dipoles in the same direction) and anti-parallel (two dipoles in the opposite direction) configurations. The magnetic field at any observation point is a vector summation of the magnetic field generated by each dipole at that point.   The distribution of magnetic fields on the x-y plane is shown in Figure 4c & 4d.   For the anti-parallel configuration, the currents are opposite for every

neighboring dipoles, therefore the magnetic fields are in the same direction between the neighboring dipoles and opposite on the other sides. In contrast, for the parallel configuration, the magnetic fields tend to cancel out each other between the dendrites and add up on the other sides.

Multi-dipole System

An image voxel typically includes millions of dendrites. We first consider that the dendrites are uniformly distributed in a voxel with parallel (all dipoles are in the same direction) or anti-parallel (any two adjacent dipoles are in the opposite direction) configurations. The distributions of magnitudes of neuronal magnetic field on the x-y plane are computed for the system and shown in Figures 5a & 5b.

Figures 5c & 5d show the changes of magnetic field along the x-axis for the parallel and anti-parallel configurations. Please note that the baseline of the magnetic field for the parallel configuration shifts with the distance. The baseline for the anti-parallel configuration approaches to zero and does not shift.

<div align="center">MRI Signal Changes</div>

MRI Magnitude Signals

The MRI signal changes depend on the strength of magnetic field as well as geometry (orientations and configurations), duration, and number of dendrites firing during the echo time. By orientation, we mean the spatial relationship between neuronal magnetic field and the B_0 field. Configuration is defined here as spatial relationship between dendrites. When all dipoles are perpendicular to the B_0 field and nuclear spins are uniformly distributed over an image voxel, the relationship between MRI signal changes and the number of dendrites firing during TE is plotted in Figure 6. Effects of

the magnitudes of intracellular current and durations of dendritic firing on msMRI signal changes are summarized in Table 1. For parallel configuration, the signal changes highly depend on the dendrites number. The msMRI signal changes could be up to 2% and are strong enough to be detected, assuming the 1 million dendrites fired, the intracellular current is 5nA and duration of each individual dendritic firing is 10ms (Table 1). For anti-parallel configuration, the signal change is very small and cannot be detected. Like MEG, msMRI signals depend on the orientation of the neuronal magnetic field. Only the component of neuronal magnetic field parallel to the B_0 can be detected. MRI signal changes reach maximum when all dipoles are perpendicular to the B_0 field. MRI signal changes approach to zero when all dipoles are parallel to the B_0 field.

MRI Phase Signals

Based on Equation 7, we can calculate the average phase change over a voxel in the same condition we described above for estimating MRI magnitude signal change. No matter whether the configuration is parallel or anti-parallel, the average phase shift for a voxel is always close to zero and undetectable when the distribution of the activated dendrites is symmetrical (Table 2). However, when the dendrites bundle is shifted away from the center of voxel, the phase distribution is no longer symmetrical to the voxel. The overall phase shift cannot be completely canceled out and is possible to be detected (Table 2-6). Figure 7 shows phase and magnitude changes induced in the voxel neighboring to the activated voxel for different number of dendrites firing in that activated voxel.

Multiple Activated Voxels

Above calculations are based on a single activated voxel. If the activated area

includes more than one voxel, the intervoxel effect must be considered. For magnitude measurement, assuming all dipoles are along the z direction with parallel configuration (see Figure 5a) and B_0 is along the y-axis, the contributions of the activated voxel to the neighboring voxel have been shown in Table 2. The activated voxel gives the largest contribution to the x neighboring voxel (85% of the signal change of the activated voxel) and the smallest contribution to the z neighboring voxel (2.5% of the signal change of the activated voxel). For phase imaging, because the phase is destructively added, the phase change for the active voxel is zero. Only in the neighboring voxel along the x-axis, the phase change may be detectable. If dipoles are in anti-parallel configuration, both the magnitude and phase changes are not detectable and can be ignored. Table 3 shows the relation between msMRI signals and the distance to the activated voxel. The contributions from the activated voxel decay rapidly.

If there are multiple voxels activated, the neuronal magnetic field of any voxel is the vector sum of the contributions from all activated voxels. Tables 4 shows both the magnitude and phase change of each voxel for two contiguous activated voxels. Tables 5 shows the magnitude and phase change of each voxel for three contiguous activated voxels. For magnitude imaging, the most sensitive voxels are on the edge of the activated area if the activated voxels are in a row along the x-axis, assuming all dendrites are in parallel configuration. The most sensitive voxel will be the voxel in the center if the activated voxels are in a row along the y- or z-axis. For phase imaging, the phase changes are approximately 0 if the activated voxels are in a row along the y- or z-axis. The phase changes are 0.57 rad if the activated voxels are in a row along the x-axis. If dendrites are in anti-parallel configuration, both the phase and magnitude signal change

are undetectable.

If the voxels are not completely occupied by activated dendrites, the partial volume effect should be considered. Assuming two contiguous activated voxels are along x, y and z directions and each of them only contains half number of dendrites, Tables 6 shows the magnitude and phase change for each voxel. For magnitude imaging, the partial volume effect is not significant in x direction. Along y and z direction, the signal changes decrease 40% and 62% respectively. The phase changes are 0.2 rad if the two activated voxels are along the x-axis. If dendrites are in anti-parallel configuration, both the phase and magnitude signal change are undetectable.

It is possible that neuronal currents in one portion of a voxel point to one direction and neuronal currents in another portion of the voxel point to the opposite direction. Table 7 shows the signal changes for a voxel in which neuronal currents in two halves are in the opposite directions. If neuronal currents in two clusters of dendrites are opposite along x direction, the overall signal change for this voxel is even larger than parallel configuration. If these two clusters are along y and z directions, the signal change is smaller than parallel configuration.

Experimental Validation

Figure 8 shows BOLD activation maps for two contiguous slices which cover primary sensory cortex (S1). Activations were found in contralateral S1 (close to BA2), primary motor cortex (M1) and the supplementary motor area (SMA).   These results are consistent with previous fMRI studies conducted with similar electrical stimulation (Backes 2000; Schulz 2004).

To assess the consistency of msMRI signal across different scan sessions, msMRI

experiments were performed on one of the subjects in three different scanning days. The activation maps for the 80ms latency component and for the control scans are shown in Figure 9. Significant activations were found close to Brodmann areas 2 (BA 2) for all three 80ms latency scans (Figure 9a-9c). Since the 80ms latency component is the late response of median nerve stimulation, the locations of the activations are closer to the anterior wall of the postcentral sulcus (BA 2), rather than the posterior wall of the central sulcus (area 3b) where the early components (N20, P30) were expected. Our results are consistent with the location of P80 potential reported by Allison (1989a). Activations were also found in some other areas (i.e. M1) but not consistent over all scans. Control scans in which no stimuli were applied were also performed for each session. As expected, the activation maps for the control scans (Figure 9d-9f) are much cleaner than the 80ms latency activation maps. Specifically, no control scan demonstrated activation in the S1 area.

Time-course plots corresponding to the activated area and the non-activated area in 80ms latency scans are shown in Figure 10. Each point on the time course was calculated by averaging 120 images. There is a significant magnitude change between baseline and activation in the activated S1 area. The mean magnitude of signal change was 0.24%. Our result is similar to the finding reported by Chow (2006a), who demonstrated a 0.15% perturbation of baseline signal in their experiment. To estimate the MRI signal change induced by fluctuation of BOLD signal, a theoretical calculation was performed to simulate BOLD effect using Gamma variate function with and without 100ms jitter. Assuming the magnitude of event related BOLD signal is 1.5%, the maximal MRI signal variation due to the fluctuation of BOLD signal is, therefore, less than 0.02%, which is

about one tenth of the msMRI signal we measured and can be safely ignored.

Identical experiments were performed on six individual subjects to assess the reproducibility of msMRI results with this paradigm across different subjects. msMRI activation maps for the 80ms latency component for these subjects are shown in Figure 11. All subjects demonstrate an S1 response in the vicinity of the posterior wall of the post central sulcus. By contrast, activations in other brain areas were not as reproducible. This inconsistency might relate to less direct temporal connection of these responses to stimulation times, or to differences in slice positions and orientations across different subjects.

Different stimulus onset asynchronies were used to explore the timing effect of msMRI. As Figure 2b and 2c show, the onsets of stimuli were adjusted to acquire the activation maps induced by different components. Figure 2b shows the timing for measuring dephasing effects of early components (0~60ms). Since there are several SEPs with opposite orientations during this time, the overall dephasing effect of these SEPs are weakened by a cancellation effect. Our result (Figure 12b) demonstrated no significant activation in the S1 area, which agrees well with our expectation. Figure 2c shows the paradigm in which the images were acquired before stimulation. No msMRI effect was anticipated in this scan. As expected, the activation maps (Figure 12c) are much cleaner than the 80ms latency activation maps. We found no activation in S1 area.

To demonstrate the TE dependence of msMRI, additional scans for TE=30, 60 and 80ms were conducted. All experiments were performed on a single subject (Subject 6) on the same day. The timing of stimulation onset was adjusted so that the center of TE (TE/2) was always located at 80ms after stimulus. Data was processed for each individual TE to

generate three activation maps (one for each TE).   A ROI was defined by combining all activated voxels in the S1 area of the three activation maps. The signal percentage changes in the ROI for TE =30, 60, 80 ms are 0.15%, 0.26%, 0.25% respectively. Figure 13 shows the simulated and experimental signal percentage change for different TEs and distributions. Since the duration of neural firing is limited (60 ms), the maximal SNR is happened when TE=60 ms. The signal changes we measured are between the simulated signal change for uniform distribution and normal distribution.

To compare both magnitude and phase effect induced by neuronal current, msMRI experiments were performed on a single subject on three different scanning days. Both magnitude and phase image were acquired at the same time. The activation maps were shown in figure 14. Significant activations were found close to primary sensory cortex (SI) (Allison 1989b) for all three scans using magnitude imaging. In contrast, activation maps for phase imaging have much less activations and no significant activation was found in SI area.
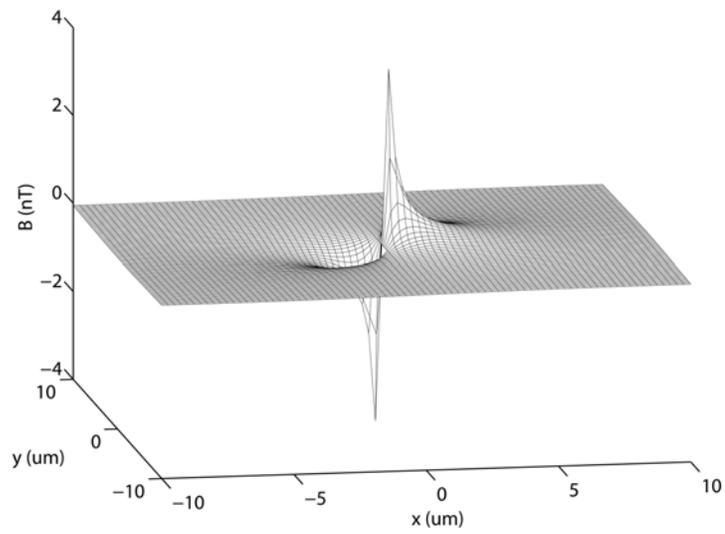
Figure 3. Magnetic field generated by neural firing for a single dendrite. The magnitude of intracellular current is 5nA and the radius of dendrite is 0.25µm.
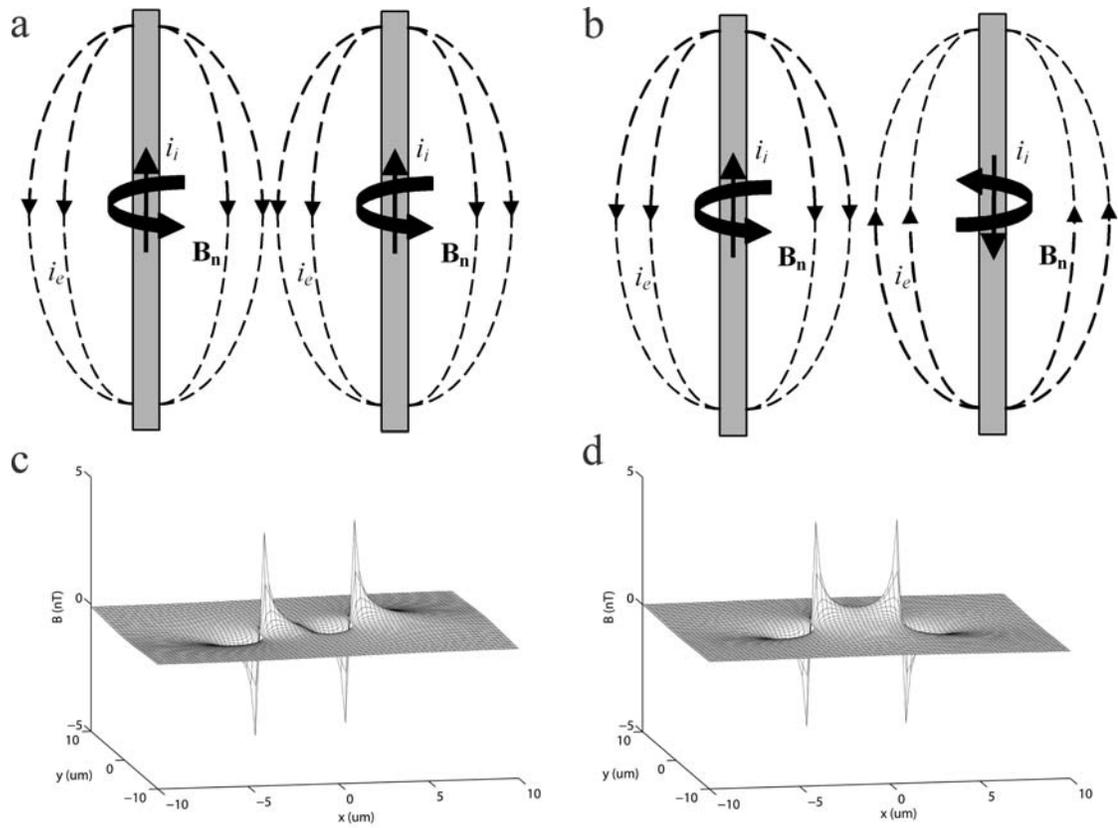
Figure 4. Configurations of a two-dipole system.
        (a) Parallel configuration
        (b) Anti-parallel configuration
        (c) Magnetic field generated by neural firing for parallel configuration
        (d) Magnetic field generated by neural firing for anti-parallel configuration
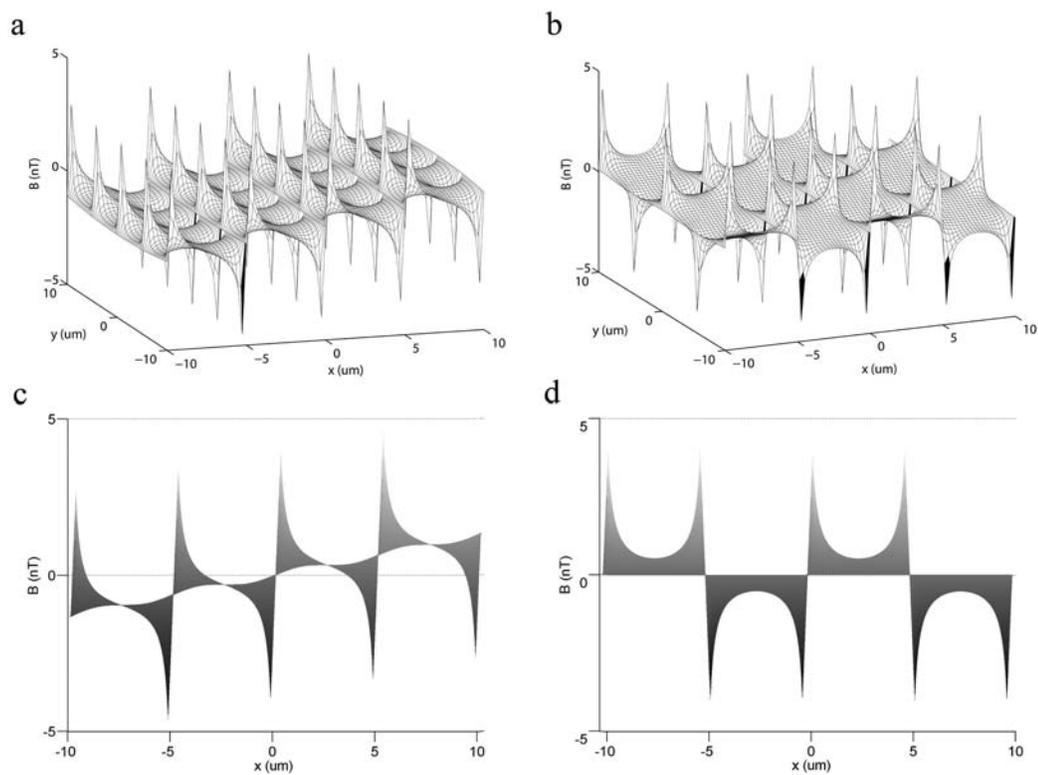
Figure 5. NMF distribution for multi-dipole system
       (a) parallel configuration
       (b) anti-parallel configuration
       (c) Magnitudes of NMF on x direction for parallel configuration
       (d) Magnitudes of NMF on x direction for anti-parallel configuration
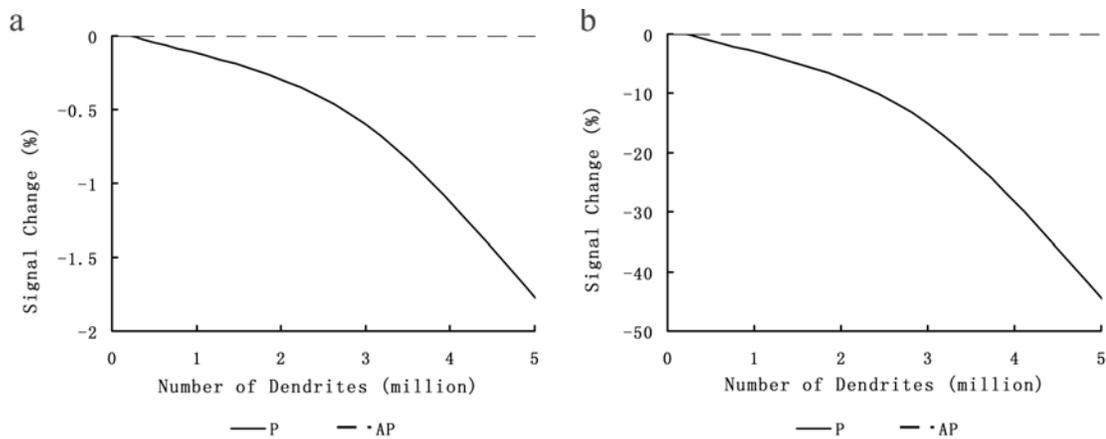
Figure 6. MRI signal changes induced by the NMF for parallel configuration and anti-parallel configuration.
(a) 1nA
(b) 5nA
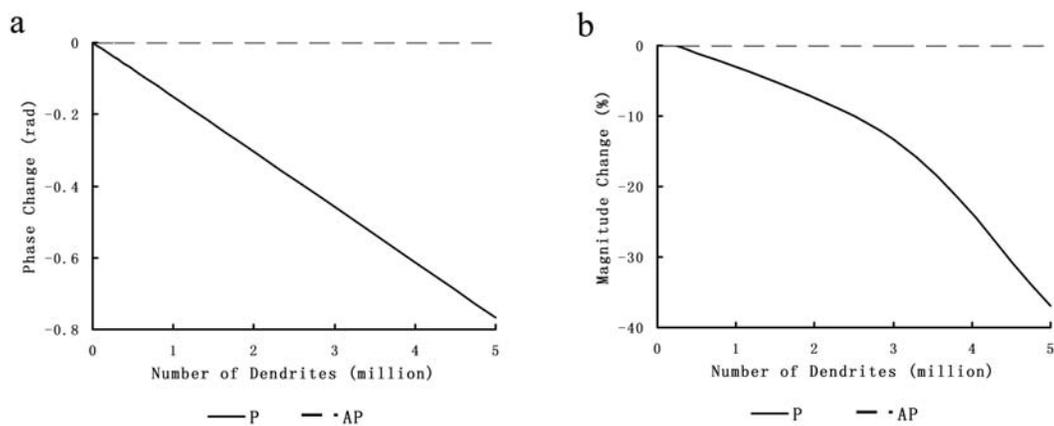
Figure 7. Phase and magnitude changes induced in the voxel neighboring to the activated
voxel for different number of dendrites firing in that activated voxel.
(a) Phase changes
(b) Magnitude changes
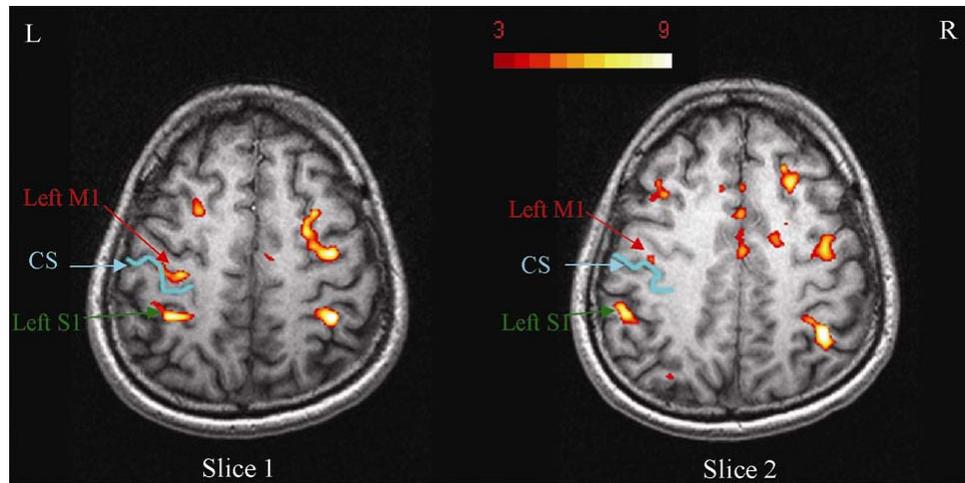
Figure 8. BOLD activation maps for two contiguous slices which cover S1 and M1 areas. Significant activation clusters were found in contralateral primary sensory cortex (S1), and primary motor cortex (M1).
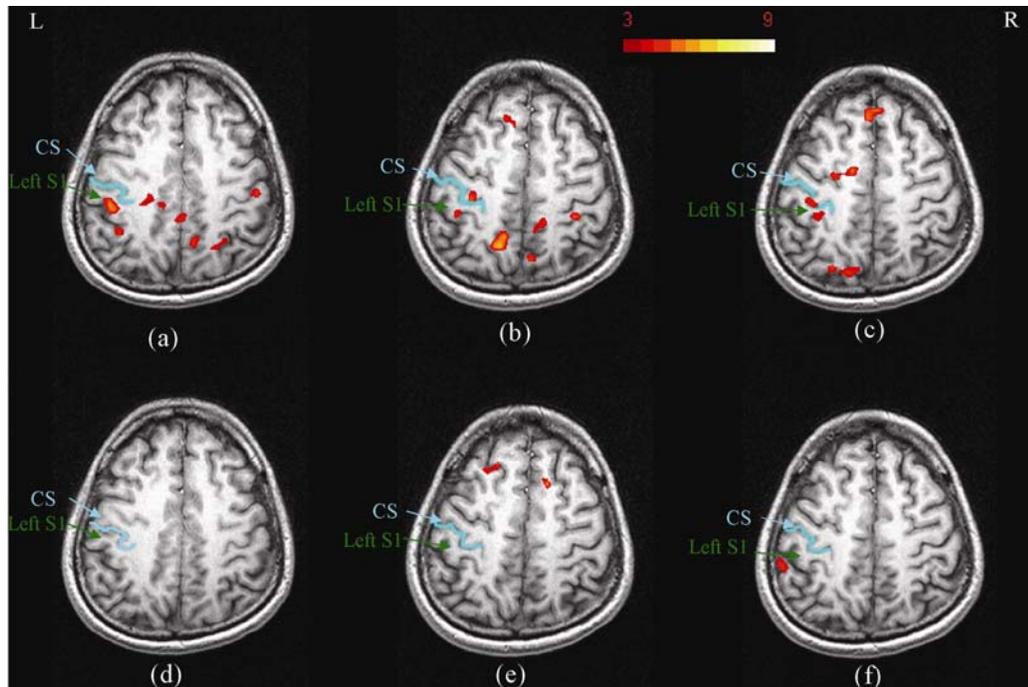
Figure 9. msMRI activation maps for single subject
(a)-(b) the msMRI activation maps of 80ms latency component for subject 1 on three different scanning days. The slice positions were manually selected to be as similar as possible. Activations in S1 were replicated.
(d)-(f) the activation maps for the control scans in which no stimuli were applied. As expected, no activation was found in area S1.
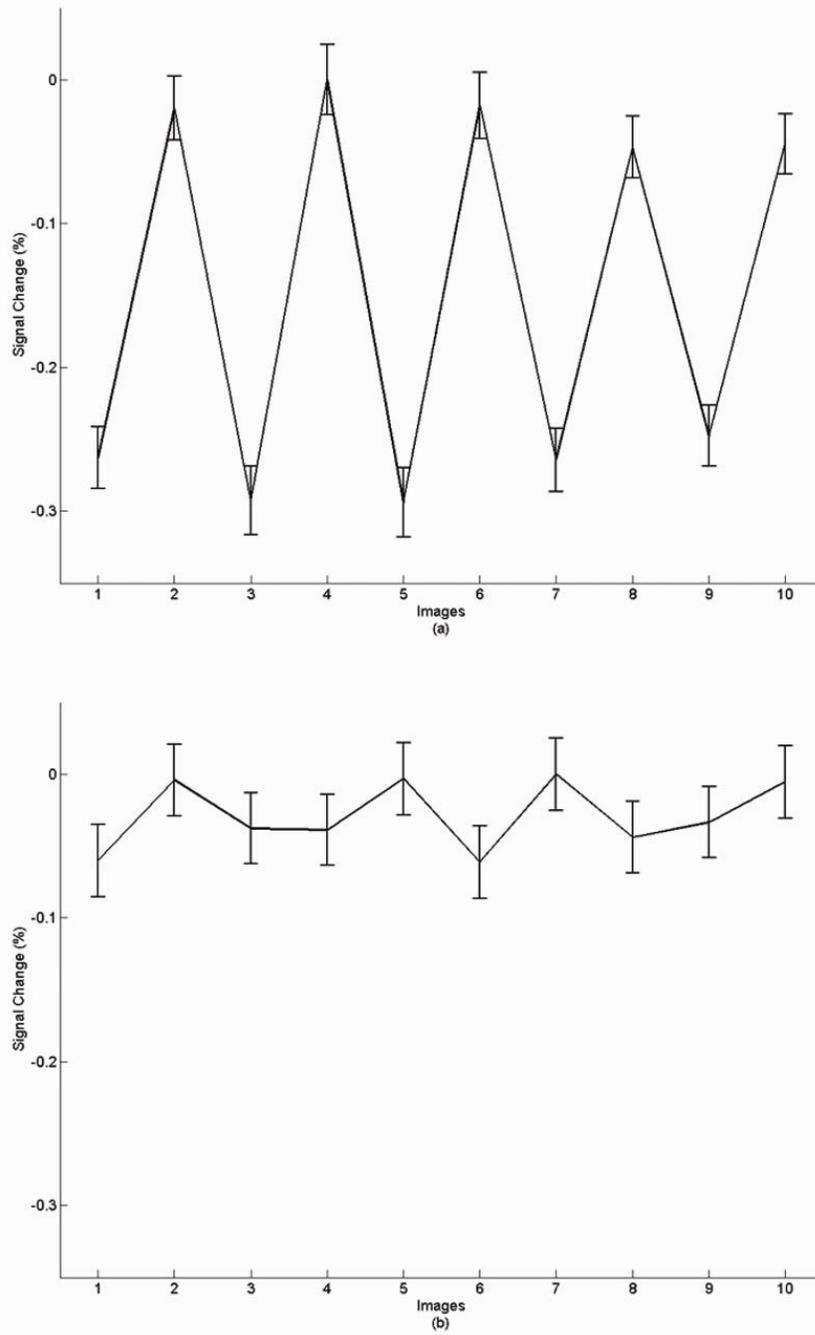
Figure 10. msMRI signal time-course plots
(a) the activated S1 area
(b) the non-activated area
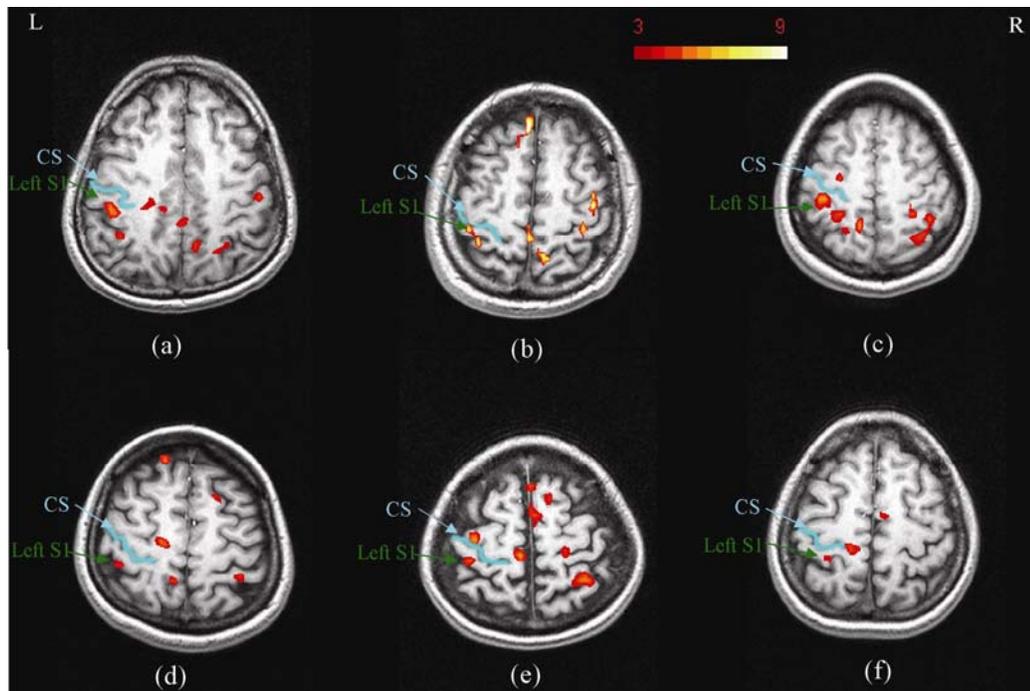
Figure 11. (a)-(f) are correspond to activation maps for subjects 1-6. All scans used an identical protocol. Activations in area S1 have good consistency across subjects, but activations in other areas (e.g. M1) have less consistency.
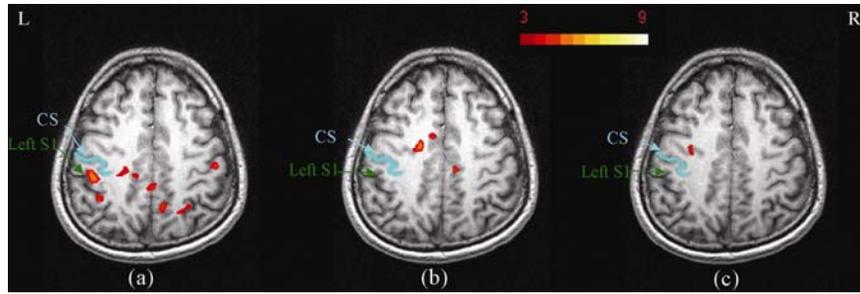
Figure 12. Activation maps demonstrating the timing effect.
(a) P80 component
(b) Early component
(c) Control scan
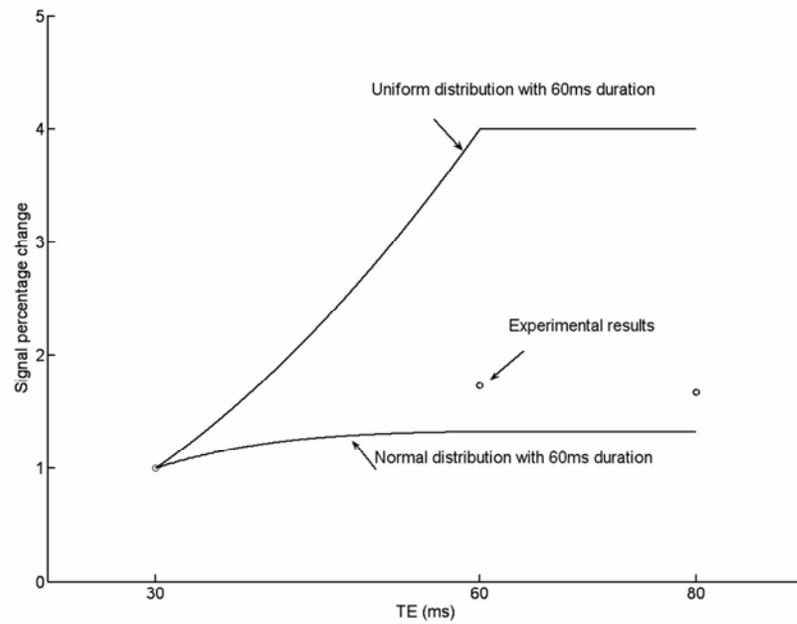
Figure 13. The signal percentage changes for different TEs and distributions. For the simulated data (solid line), a limited duration (60ms) of neuronal activity was assumed. No opposite neuronal magnetic field was considered. All data were normalized to TE=30ms. The TE was centered at P80 component (TE/2 was located at 80ms after stimulus).
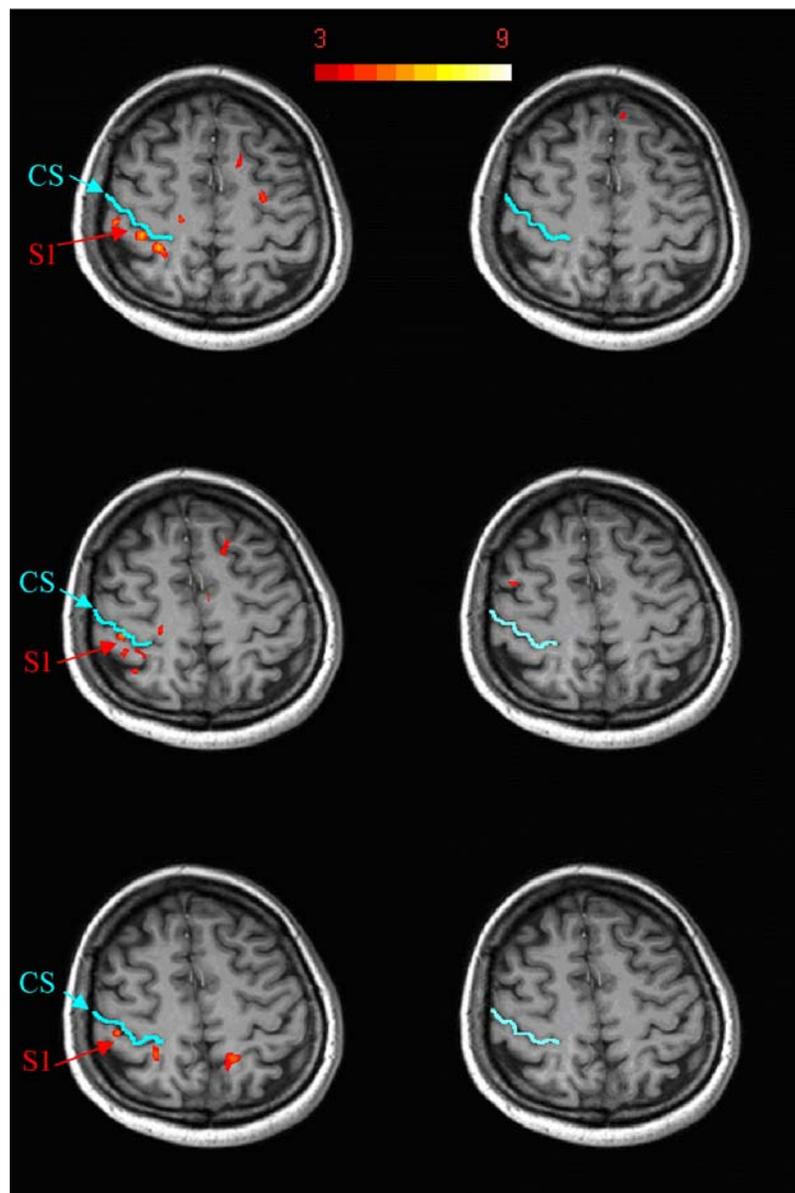
Figure 14. msMRI activation maps for a single subject on three different scanning days. Left column are magnitude images. Right column are phase images.

Table 1. MRI Magnitude Signal Changes of the Activated Voxel Corresponding to Different Parameters of Neural Firing

Neuronal Current	Configuration	5 ms	10 ms
1nA	Parallel	-0.02%	-0.08%
	Anti-Parallel	-1.3×10^{-8}	-5×10^{-7}
5nA	Parallel	-0.49%	-2.0%
	Anti-Parallel	-3.2×10^{-7}	-1.3×10^{-6}

Note: One million dendrites fired during the TE (100ms). The radius of dendrite is 0.25μm. The results in this table are MRI magnitude signal changes. Phase signal changes are close to zero in any situations.

Table 2. The msMRI Signal Changes of an Activated Voxel and Its Neighboring Voxels Along the x, y and z Directions

	Configuration	Activated voxel	X neighbor	Y neighbor	Z neighbor
Magnitude changes	Parallel	-2.0%	-1.7%	-0.16%	-0.05%
	Anti-Parallel	-1.3×10^{-6}	0	0	0
Phase changes	Parallel	0	0.17 rad	0	0
	Anti-Parallel	0	0	0	0

Note: The parameters for this computation are: The duration of each individual dendritic firing is 10ms, the magnitude of intracellular current is 5nA, and the radius of dendrite is 0.25µm and 1 million dendrites fire during TE (100ms).

Table 3. The msMRI Signal Changes of An Activated Voxel and Its Neighboring Voxels Along the x Directions

	Activated voxel	First neighbor	Second neighbor	Third neighbor	Forth neighbor
Magnitude changes	-2.0 %	-1.7%	-0.09%	-0.02%	-0.005%
Phase changes	0	0.17 rad	0.042 rad	0.018 rad	0.011 rad

Note: The parameters for this computation are: The duration of each individual dendritic firing is 10ms, the magnitude of intracellular current is 5nA, the radius of dendrite is 0.25µm and 1 million dendrites are considered firing during TE (100ms). All dipoles in the activated voxel are in parallel configuration.

Table 4. The msMRI Signal Changes of Two Contiguous Activated Voxels Along the x, y, and z Directions

	Configuration	X	Y	Z
Magnitude changes	Parallel	Voxel 1: -2.1% Voxel 2: -2.1%	Voxel 1: -3% Voxel 2: -3%	Voxel 1: -2.6% Voxel 2: -2.6%
	Anti-Parallel	-1.3×10^{-6}	-1.3×10^{-6}	-1.3×10^{-6}
Phase changes	Parallel	Voxel 1: -0.17 rad Voxel 2: 0.17 rad	0	0
	Anti-Parallel	0	0	0

Note: The parameters for this computation are: The duration of each individual dendritic firing is 10ms, the magnitude of intracellular current is 5nA, the radius of dendrite is 0.25μm and 1 million dendrites are considered firing during TE (100ms) for each voxel.

Table 5. The msMRI Signal Changes of Three Contiguous Activated Voxels Along the x, y, And z Directions

		X	Y	Z
Magnitude changes	Parallel	Voxel 1: -2.7% Voxel 2: -0.07% Voxel 3: -2.7%	Voxel 1: -3.2% Voxel 2: -4.2% Voxel 3: -3.2%	Voxel 1: -2.8% Voxel 2: -3.5% Voxel 3: -2.8%
	Anti-Parallel	-1.3×10^{-6}	-1.3×10^{-6}	-1.3×10^{-6}
Phase changes	Parallel	Voxel 1: -0.2 rad Voxel 2: 0 Voxel 3: 0.2 rad	0	0
	Anti-Parallel	0	0	0

Note: The parameters for this computation are: The duration of each individual dendritic firing is 10ms, the magnitude of intracellular current is 5nA, the radius of dendrite is 0.25μm and 1 million dendrites are considered firing during TE (100ms) for each voxel.

Table 6. The msMRI Signal Changes for Each Activated Voxel due to the Partial Volume Effect

	Configuration	Activated voxel	X	Y	Z
Magnitude changes	Parallel	-2.0%	-2.4%	-1.2%	-0.76%
	Anti-Parallel	-1.3×10^{-6}	-0.7×10^{-6}	-0.7×10^{-6}	-0.7×10^{-6}
Phase changes	Parallel	0	0.2 rad	0	0
	Anti-Parallel	0	0	0	0

Note: The parameters for this computation are: The duration of each individual dendritic firing is 10ms, the magnitude of intracellular current is 5nA, and the radius of dendrite is 0.25μm and 1 million dendrites fired during TE (100ms). We consider two contiguous activated voxels are along x, y and z directions respectively. Only half volume of each voxel contains dendrites.

Table 7. The Signal Changes for a Voxel In Which Neuronal Currents In Two Halves are In the Opposite Directions

	Configuration	Activated voxel	X	Y	Z
Magnitude changes	Parallel	-2.0%	-3.6%	-0.4%	-0.7%

Note: The parameters for this computation are: The duration of each individual dendritic firing is 10ms, the magnitude of intracellular current is 5nA, and the radius of dendrite is 0.25μm and 1 million dendrites fire during TE (100ms). In each voxel, neuronal currents in one portion of a voxel point to one direction and neuronal currents in another portion of the voxel point to the opposite direction. Here, we consider these two portions are along x, y and z directions respectively.

CHAPTER V

DISCUSSION AND CONCLUSION

<u>Theoretical Modeling</u>

In this work, we present a modified dipole model to estimate the magnetic field induced by neuronal firing. Each branch of dendrite and each axon of a neuron have been modeled using a modified dipole model. Effects of geometry and density of the synchronously firing neurons on MRI signal changes have been investigated. Our modeling indicates that magnitude msMRI is more sensitive for detecting the neuronal magnetic field than phase msMRI.

<div align="center">Synchronized vs Unsynchronized Neural Firing</div>

While both msMRI and MEG detect the neuronal magnetic field, they focus on different properties of the field. MEG measures the strength of the neuronal magnetic field, which is a vector summation of the magnetic fields generated by all individual dendrites firing simultaneously. Synchronized firing is the key to generate a strong and detectable magnetic field for the MEG measurement. On the other hand, msMRI signals, either msMRI phase imaging or msMRI magnitude imaging, are originated from phase changes experienced by individual spins. The phase changes are accumulated effects of the neuronal magnetic field during the echo-time, TE. All neural firings during TE will contribute to the dephasing of the proton spins and cause MRI signal change, no matter whether these neurons fire simultaneously or not. In other words, msMRI signals depend on the total number of neurons fired during TE and are independent of temporal relation (sequence) of neural firings.

Effects of Dendritic Parameters

Dendritic parameters, such as number of dendrites, physical sizes of dendrites, and firing patterns, strongly affect the neuronal magnetic field distribution. Their influences on msMRI signals need to be investigated. Because of measuring accumulated effects of the neuronal magnetic field, msMRI signals do not directly depend on the magnitude, duration, and shape of neuronal currents. As long as time integrals of neuronal currents are the same, changes in magnitude, duration, and shape do not affect msMRI signals at all. Thus greatly simplify our modeling because those parameters vary over a large range, depending on the branch order, passive and active property of dendrites. In this work, we simplify dendritic currents as a rectangle waveform with magnitudes varying from 1nA to 5nA and durations from 5ms to 10ms (Destexhe 1998; Williams 2002; Gulledge 2005), radius of dendrite: 0.25 μm to 0.5 μm (Weaver 2004), length of dendrite branch: 1 mm (Weaver 2004; Gulledge 2005), intracellular current: 1nA to 5nA (Destexhe 1998), and duration of each individual dendritic firing: 5 ms to 10 ms (Williams 2002; Gulledge 2005).

The physical sizes of dendrites are relatively easy to be estimated. Base on literature, the average radius of dendrites is about 0.25 μm to 0.5 μm (Weaver 2004). The average length of dendrite branch is approximately 1 mm (Weaver 2004; Gulledge 2005). The most difficult parameter to be estimated is the number of dendrites fired during TE. An unbiased estimate (Schumann 2005) is roughly 7 million neurons for a typical fMRI voxel of 3x3x3 mm^3. Based on the MEG literature (Cohen 1968; Hamalainen 1993), the evoked magnetic fields on the scalp (2-4 cm away from the current source) are in the order of $\Delta B=10^{-13}$ T. It has been assumed that a large number of neurons (50,000 or

more) occupying an area of a few mm^2 must fire simultaneously to generate such a field

(Hamalainen 1993; Romani 1989). The number of simultaneously fired neurons is then

roughly 1% of the total neurons in the voxel. This number (50,000) should be the number

of neurons fired at a particular time. Because msMRI technique measures the

accumulated effect of neuronal magnetic field, all the dendrites firing during TE will

contribute to the dephasing of spins. The typical temporal width of the neuronal magnetic

field peak is on the order of 100 msec. To create this non-stop current, multiple dendrites

have to fire sequentially. If the duration for single neuron firing is from 5ms-10ms, there

are 0.5 million to 1 million neurons firing during TE. With tens to thousands of

synapses for each neuron (Lewine 1995), a reasonable estimation for the number of

dendrites firing during TE should be up to several millions. The msMRI signals generated

by such number of activated dendrites should be strong enough to be detected using

current MRI techniques.

<div align="center">Effects Of Dendrite Configurations</div>

All our analyses are based on the assumption of rather simple configurations of

dendrites: parallel or anti-parallel configurations. The real configurations of dendrites in

the brain should be much more complex. Let us first rotate every other dipole in

Figures 5a, 5b by an angle α. Assume that all dipoles in Figures 5a, 5b are

perpendicular to the B_0 field. If the dipoles being rotated are still perpendicular to the

B_0 field, MRI signal changes are in the range defined by the parallel (the upper limit) and

the anti-parallel configurations (the lower limit) (Figure 6). If the dipoles being rotated

are no longer perpendicular to the B_0 field, MRI signal changes will decrease. In the

worst case where the rotated dipoles are parallel to the B_0 field, majorities of neuronal

magnetic field generated by the rotated dipoles are perpendicular to the B_0 field. The msMRI signal changes will decrease by almost 50%.

When all dipoles are perpendicular to the B_0 field, the upper and lower limits of msMRI signals are defined by the parallel and anti-parallel configurations. Whether or not the msMRI signals are detectable in real situation depends on how many activated dendrites are in parallel, rather than anti-parallel, configuration. As we all know, anti-parallel configuration generates no detectable signals outside the brain. The factor that MEG can detect neuronal magnetic signals implies that parallel configuration plays an important role. The number of coherently activated neurons (50,000 or more) estimated based on MEG literature (above) should be neurons in parallel configuration. As we discussed in the previous section, detectable msMRI signals could be expected.

It is also possible that neuronal currents in one portion of a voxel point to one direction and neuronal currents in another portion of the voxel point to the opposite direction. We choose to discuss a simple example in this revision, i.e., neuronal currents in half voxel point to one direction and neuronal currents in another half point to the opposite direction. As shown in Table 7, when neuronal currents in two clusters of dendrites are opposite along x direction, the magnetic fields add up between these two clusters of dendrites. Therefore, the overall signal changes for this voxel is larger than parallel configuration. If these two clusters are along y and z directions, the magnetic fields may cancel out each other and result in smaller signal changes. Our results demonstrate that although the net number of neurons with parallel configuration is zero (half dendrites are in one direction and half dendrites are in the opposite direction), the signal changes still can be detected in some cases.

Phase vs Magnitude

Depending on magnetic field distribution, neuronal activity may be detected as phase or magnitude changes of MRI signals. MRI phase imaging measures phase shift of nuclear spins which depends on the average strength (averaged across an image voxel) of neuronal magnetic field. In contrast, MRI magnitude imaging measures phase dispersion which is the variation (or local inhomogeneity) of neuronal magnetic field. The magnetic field induced by neuron firing is highly inhomogeneous. As shown in Figure 1a, the magnetic field on the right side of the dipole is always opposite to that on the left side. Thus, phases of nuclear spins located on the right side of the dipole are also always opposite to those on the left side. A typical MRI voxel consists of millions of such dipoles. Phase of MRI signal, which represents the overall phase shift of all spins in the voxel, tends to be destructively added and is approximately zero. Phase measurements are therefore insensitive for detecting neuronal magnetic field. On the other hand, neural activity will increase the fluctuations of magnetic fields and increase phase dispersion of nuclear spins. This phase dispersion will result in a decrease of MRI magnitude signal during brain activation. Hence, the magnitude measurements should be more sensitive than phase measurements.

While we argue that phase measurements are insensitive for detecting neuronal magnetic field in the activated voxel, it could be detectable in some situations. When the dendrites bundle is shifted away from the center of voxel along x direction, the overall phase shift cannot be totally canceled out. In this situation, phase measurements could be achievable (Table 2-6). In addition, phase detection is also possible in the voxels neighboring to the activated voxel in the x-direction. This result is consistent with the

previous modeling (Konn 2003) which reported that the largest image contrast is always achieved in a voxel neighboring the active cortical tissue. However, in other two directions (y and z directions), the phase signal changes are always destructively added and cannot be detected. In contrast, magnitude imaging has no such limitations. As demonstrate by Table 2-7, magnitude signal changes are detectable no matter the distribution of the activated dendrites is symmetrical or not.

<div align="center">Multiple Activated Voxels</div>

Contributions of an activated voxel on its neighbors are anisotropic. As shown in Table 2, the largest contribution is on the x-axis direction and the smallest contribution is on the z-axis direction. When multiple voxels are activated, the neuronal magnetic field of any voxel is a vector summation of magnetic fields from all activated voxels. Because different contributions of an activated voxel to its different neighbors, msMRI signal changes depend strongly on configurations of the activated voxels. For two contiguous activated voxels, the signal changes are the same for both voxels and are larger than that for a single activated voxel (Table 4). Although contribution of an activated voxel to its x-axis neighbor is the largest, part of magnetic field generated by the neighbor will be destructively added with magnetic field generated by the voxel. The overall magnitude signal changes are almost same as the signal change for a single activated voxel. In y and z direction, the contributions from neighboring voxel always have same direction with the magnetic field itself. Therefore, the overall magnitude signal changes for each voxel is larger than that for a single activated voxel. For three contiguous activated voxels, the signal changes are not identical for the three voxels anymore (Table 5). In x direction, the signal changes for the voxels at the edge are

much larger than the voxel in the center because magnetic fields from the two neighboring activated voxels will partly cancel out magnetic field generated by the center voxel. However, in y and z direction, the magnetic fields from the neighboring activated voxels are constructively added with the magnetic field generated by the center voxel, resulting in the largest change for the central voxel. For phase imaging, because the activated voxels are only contributed to the voxels along x direction, only the signal changes along x direction may be detectable.

If only half volume of voxels contains dendrites, the signal changes should decrease correspondently. However, if the contribution from the neighboring activated voxel which also contains the half number of dendrites is considered, the signal changes do not decrease too much along y and z directions and can even increase along x direction (Table 6).

The above discussed are valid for the parallel configuration only. For anti-parallel configuration, there are no signal changes can be detected, regardless either phase imaging or magnitude imaging is used.

<center>Diffusion Effect</center>

For anti-parallel configuration, the dominant fields are fast decayed magnetic fields (Figure 5d). Since these fast decayed magnetic fields are spatially limited, their effects on nuclear spins are typically small, no matter whether diffusion effects are considered. Based on literature, the average apparent diffusion coefficient (ADC) of water in cortex is 0.676×10^{-3} mm^2/s for 3D isotropic diffusion (Darquie 2001). The average diffusion distance of water molecules is then about 20 μm within TE (100 ms). This distance is far larger than physical dimensions of the fast decayed magnetic fields (about 2 μm, Figure

5d). The water molecules may sample both positive and negative magnetic fields and result in an even smaller net neuronal magnetic field effect when diffusion is considered (Weisskoff 1994). For parallel configuration, the magnetic field can be treated as a combination of multiple rapidly changing magnetic fields and a slowly shifting baseline magnetic field (Figure 5c). When the diffusion effects are considered, contributions of the rapidly changing magnetic fields to the msMRI signals are approximately 0. Since the physical size of the slowly shifting baseline magnetic field (several millimeters) is much larger than the diffusion distance, diffusion effects can be evaluated by equation $S = S_0 e^{-bD}$, where S is measured signal, S_0 is signal without diffusion effect, b is b factor, and D is diffusion coefficient. The b factor is proportional to the square of gradient strength. Based on our model, the maximal gradient strength generated by neuronal currents is on the order of 10^{-2} mT/m which is at least 3 orders lower than the gradient strength commonly used in EPI pulse sequences. Even for a long TE (100ms), the overall diffusion effect of the neuronal magnetic field is still very small. Because the baseline shifting magnetic field is a dominant factor for the parallel configuration, diffusion effects on the msMRI signals are then insignificant.

<div align="center">Model Limitations</div>

While our modeling is instrumental for our understanding of the mechanism of msMRI signal, there are several limitations. The first limitation of our combined model is the assumption of rather simple configurations of dendrites: parallel or anti-parallel. A more accurate model of the configuration of dendrites is needed to better predict MRI signal. The second limitation of the model is the assumption of a uniform distribution of dendrites in a voxel. Yet, the distributions of dendrites are not uniform in the brain.

A more realistic model is in development to address all above-mentioned problems.

In summary, our results indicate that MRI signal changes induced by neuronal magnetic field are in the detectable range of current MRI techniques. Magnitude measurements are more sensitive for detecting *in-vivo* neuronal activity than phase measurements in some situations. Our work demonstrates the feasibility of direct MRI detection of neuronal activity and will provide a theoretical background for future developments, optimizations, and applications of the technique.

<u>Experimental Validation</u>

In experimental validation work, we present a rapid median nerve stimulation paradigm for the detection of msMRI signal. Our initial results are demonstrating a consistent 80 ms latency activation of the primary somatosensory cortex, within subject and across subjects. Earlier components were not detected, consistent with the expected cancellation effect of bi-polar neuronal magnetic fields. As expected, the magnitude of the msMRI signal was 0.2%~0.3%.

Consistency

As our results indicate, msMRI contrast is much weaker than BOLD contrast. Despite the small magnitude of the signal, it is consistently present. In subject 1, S1 activation was demonstrable in each of three sessions, conducted on different scanning days (Figure 9). Significant activations were found in S1 and M1 areas in 80ms latency scans. No such activations were seen in these areas in the control scans on each date. The result was also consistent across subjects. S1 was activated in each of the six individuals, implicating a sector of the anterior wall of the postcentral sulcus (Figure 11). Activations in other brain areas were not very consistent across different subjects and

different sessions for the same subjects. Possible reasons for such inconsistency include: (1) Variations in slice incidence and location. In our experiments, the slice positions were manually selected to be as similar as possible for each repeat scan, but the slice orientation and position can not be identical. (2) The temporal TE window we selected in our experiment was optimized to detect the activity in area S1. The activities in other areas linked to other or variable times would not be detected as well. (3) The slice position was targeted on area S1. The activations in other areas will be missed if they are not in the same slice. (4) The responses in other areas may have a larger variance in both timing and magnitude across subjects. For example, even though the activations in SMA can be clearly identified in BOLD results, it has been reported that no ERPs can be detected in this area (Kakigi 1994). Further studies are required to clarify this issue.

<div align="center">Timing Effect</div>

msMRI is a technique with high temporal resolution. It is thus quite sensitive to the onset and offset of stimulus. Different components of neuronal responses are measured by using different SOAs. In our experiments, three different SOAs (-50 ms, 0 ms and 100 ms relative to the trigger from scanner) were used in msMRI scans to measure the dephasing effect of different components. Our results demonstrated that neural responses with different latencies had different dephasing effects. The 80 ms latency component is a relatively long response that doesn't change orientation (sign) during TE. The overall msMRI contrast, therefore, will be maximized since msMRI measured an accumulated dephasing effect during TE. In contrast, early components (0~60 ms) include several SEPs with opposite orientations (signs) that are spatially proximate to each other, e.g. in adjacent banks of the central sulcus. The dephasing effects will be canceled out and make

these components undetectable. This notion is consistent with our results (Figure 12b). When the target slice was acquired 100ms before the stimuli were applied, no dephasing effect was anticipated. As expected, there are no activations found in S1 area (Figure 12c). Bianciardi (2004) reported similar temporal property. They used spin echo sequence to reverse the dephasing effect from the opposite neuronal magnetic fields and minimized the cancellation effect. In short, gradient echo sequence is suitable to detect the neuronal current effect without sign change. In contrast, spin echo sequence may be a good choice for neuronal magnetic field with sign change. The timing property supports our claim that the activations we detected were most likely from neuronal current effects rather than hemodynamic response.

msMRI vs. BOLD Contrast

Neuronal activity induces not only neuronal magnetic field, but also a change of blood flow or blood oxygenation level. Thus it needs to be discussed whether our activations were actually due to msMRI contrast or perhaps to BOLD effect or noise. We believe the results we reported are indeed msMRI effects, for the following reasons. (1) In this study, we used a high stimuli presentation rate to drive the BOLD response to steady state. BOLD response was saturated in the steady state in this case. All the data were acquired during this steady state phase. Further, each trial consists of one activation image and one control image. The activation state is directly compared to the control state. Any signals common for both the control and the activation images were removed. Since each trial was acquired with very short interval (600 ms), the slowly changing BOLD effect and other physiological noises were better suppressed. The BOLD contribution is less than 0.02%, based on our simulations. The signal from neuronal currents, therefore,

should be the dominant signal. (2) msMRI has a high temporal resolution and is very sensitive to the timing of stimulation. Different SOAs may generate complete different results. The BOLD response, however, is slow and long lasting, and much less sensitive to the SOAs. In addition, BOLD contrast has no such cancellation effect since the blood oxygenation level always increases when neurons are activated. Therefore, the strong SOA dependence of our results strongly suggests that the activations we found were induced by neuronal magnetic fields rather than BOLD effects.

A long ISI design was also performed for this study. A pretty long ISI (19.8 sec) was used to allow the BOLD signal return to baseline. Most contribution from the BOLD effect was eliminated. However, this design is not very time efficient. Only 18 pairs (18 controls and 18 activations) of data were collected in a 6-min long scan. No significant activation was found in S1 area. The reason, we believe, is that the SNR is not high enough for detecting neuronal signals. For comparison, we collected 600 pairs of data in our short ISI design. It would take an extremely long scan session (hours) to achieve a similar SNR for the long ISI design. Similar discussion and conclusion have been presented in Hagberg 's paper (2006).

Optimal TE

As we stated in the method section, TE selection depends on 1) T2* values 2) duration and shape of the neuronal magnetic field. For an infinitely long and uniformly distributed activation, the optimal TE is two times T2* of the tissue. When the duration of activation is limited and the shape of neuronal magnetic field is not uniformly distributed, the optimal TE is less than two times T2*. In this study, the P80 component lasts about 60ms (Allison 1989b). A long TE (>60ms), therefore, would not increase signal

percentage change but result in a lower SNR. The signal percentage change for TE=80 ms is 0.25% which is similar to the signal percentage change for TE=60 ms (0.26%). Moreover, the real distribution of fired neurons are not uniformly distributed during TE. Thereby we chose TE=60 ms in this study.

<div align="center">msMRI CNR</div>

A previous MEG study (Kakigi 1994) has reported that the evoked magnetic fields on the scalp (2-4 cm away from the current source) are on the order of $\Delta B=10^{-13}$ T. It could be assumed that at least 50,000 or more cortical neurons that occupy an area of a few mm^2 must fire simultaneously and coherently to generate such a field strength (Romani 1989; Hamalainen 1993). Since msMRI measures the accumulated effect of neuronal magnetic field, the overall signal changes induced by neuronal magnetic field during TE (60 ms used in this study) could be 0~0.7% based on the model of Xue (2006). It should be noted that 0.7% is the signal change for the extreme situation (all dipoles are in the same direction). For real application, the signal change should be smaller than 0.7%. From our experiment results, we found a 0.2%~0.3% signal change, which is in the range of the signal change predicted above.

To increase CNR, a total of 1200 images, 5-10 times more than conventional BOLD fMRI, were acquired to improve the statistic power. By taking account of the lower magnitude of msMRI signal and lower flip angle we used in this experiment, the overall CNR is about five times lower than BOLD imaging. Nevertheless, it is still possible for current MRI techniques to detect the activation. Besides system noise, some other sources of noise could also potentially lower the CNR and decrease msMRI signal detectability. Physiological noise, such as heartbeat (1.1-1.4 Hz) and respiration (0.15-0.25 Hz), is

significant for experiments aiming at detecting neuronal currents by MRI. Our simulation rate was chosen as 1.67 Hz to avoid these physiological frequencies. A temporal high pass filter was applied to minimize the physiological noises. In addition, since each slice was acquired at a different time, any interpolations between the slices could be avoided. CNR, therefore, will suffer from the movement of the subjects, especially in longitude direction.

<div align="center">Magnitude and Phase Effect</div>

Both magnitude and phase changes induced by neuronal current have been measured to detect the dephasing effect induced by neuron activity. However, which method is more sensitive is still a matter of debate. Phase imaging measures the average of phase shift across an image voxel. If the activated neurons are located at the center of voxel, the phase of MRI signal tends to be destructively added and is approximately zero since the magnetic field on the opposite side of the dendrites are always opposite. When the neuronal magnetic field is not symmetrically distributed in the voxel, the net phase change can be generated. However whether this change strong enough to be detectable is still debate. In contrast, MRI magnitude imaging measures the variation of neuronal magnetic field. The phase dispersion induced by neuron activity will always result in a decrease of MRI signal. Hence, the magnitude imaging should be more sensitive than phase imaging. This is well agreed with our finding.

In summary, this study shows a transient and weak, but consistent task-induced msMRI signal detected in S1 by msMRI. The magnitude change of MRI signal was around 0.2~0.3%. The intrinsic temporal sensitivity of msMRI technique is demonstrated. This temporal sensitivity must be respected in experimental design.

While we demonstrated msMRI signal is in the detectable range of current fMRI technique, CNR is still much lower than BOLD imaging. Further work is required to improve experiment design and CNR to confirm our findings.

BIBLIOGRAPHY

Allison, T. 1989a. Human cortical potentials evoked by stimulation of the median nerve. I. Cytoarchitectonic areas generating short-latency activity. J Neurophysiol 62: 694-710.

Allison, T. 1989b. Human cortical potentials evoked by stimulation of the median nerve. II. Cytoarchitectonic areas generating long-latency activity. J Neurophysiol 62: 711-722.

Backes, W.H. 2000. Somatosensory cortex responses to median nerve stimulation: fMRI effects of current amplitude and selective attention. Clin Neurophysiol 111: 1738-1744.

Bandettini, P.A. 1992. Time course EPI of human brain function during task activation. Magn. Reson. Med. 25, 390-397.

Belliveau, J.W. 1991. Functional mapping of the human visual cortex by magnetic resonance imaging. Science 254, 716-719.

Bianciardi M. 2004. Combination of BOLD-fMRI and VEP recordings for spin-echo MRI detection of primary magnetic effects caused by neuronal currents. Magn Reson Imaging 22: 1429-1440.

Blagoev, K.B. 2007. Modelling the magnetic signature of neuronal tissue. NeuroImage 37: 137-148.

Bodurka, J. 1999. Current-induced magnetic resonance phase imaging. J Magn Reson 137: 265-271.

Bodurka, J. 2002. Toward direct mapping of neuronal activity: MRI detection of ultraweak, transient magnetic field changes. Magn Reson Med 47: 1052-1058.

Cassara, A.M. 2008. Realistic simulations of neuronal activity: A contribution to the debate on direct detection of neuronal currents by MRI. NeuroImage 39:87-106.

Chow, L.S. 2006a. Investigating direct detection of axon firing in the adult human optic nerve using MRI. Neuroimage 30: 835-846.

Chow, L.S. 2006b. Investigation of MR signal modulation due to magnetic fields from neuronal currents in the adult human optic nerve and visual cortex. Magn Reson Imaging 24: 681-691.

Chu, R. 2004. Hunting for neuronal currents: absence of rapid MRI signal changes during visual-evoked response. NeuroImage 23: 1059-1067.

Cohen, D., 1968. Magnetoencephalography: evidence of magnetic fields produced by alpha-rhythm currents. Science 161: 784-786.

Darquie, A. 2001. Transient decrease in water diffusion observed in human occipital cortex during visual stimulation. Proc Natl Acad Sci USA 98: 9391-9395.

Destexhe, A. 1998. Dendritic low-threshold calcium currents in thalamic relay cells. J Neurosci 18: 3574-3588.

Fox, P.T. 1986. Focal physiological uncoupling of cerebral blood flow and oxidative metabolism during somatosensory stimulation in human subjects. Proc Natl Acad Sci USA 83: 1140-1144.

Gulledge, A.T. 2005. Synaptic Integration in Dendritic Trees. J Neurobiol 64: 75-90.

Hagberg G.E. 2006. Challenges for detection of neuronal currents by MRI. Magn Reson Imaging 24:483-493.

Hamalainen, M. 1993. Magnetoencephalography − theory, instrumentation, and applications to noninvasive studies of the working human brain. Rev Mod Phys 65: 413-497.

Kakigi, R. 1994. Somatosensory evoked magnetic fields following median nerve stimulation. Neurosci Res 20: 165-174.

Kamei, H. 1999 Neuronal Current Distribution Imaging Using Magnetic Resonance. IEEE Trans Magn 35: 4109-4111.

Konn, D. 2003. MRI detection of weak magnetic fields due to an extended current dipole in a conducting sphere: a model for direct detection of neuronal currents in the brain. Magn Reson Med 50: 40-49.

Kwong, K.K. 1992. Dynamic magnetic resonance imaging of human brain activity during primary sensory stimulation. Proc Natl Acad Sci USA 89: 5675-5679.

Lai, S. 1993. Identification of vascular structures as a major source of signal contrast in high resolution 2D and 3D functional activation imaging of the motor cortex at 1.5T: preliminary results. Magn Reson Med 30: 387-392.

Lewine, J. 1995. Clinical electroencephalography and event-related potentials. In: Functional Brain Imaging, edit by W. Orrison. St. Louis: Mosby-Year Book, Inc.

Liston, A.D. 2004. The MR detection of neuronal depolarization during 3-Hz spike-and-wave complexes in generalized epilepsy. Magn Reson Imaging 22: 1441-1444.

Norris, D.G. 2003. High Field Human Imaging. J Magn Reson Imaging 18: 519-529.

Ogawa, S. 1992. Intrinsic signal changes accompanying sensory stimulation: functional brain mapping with magnetic resonance imaging. Proc Natl Acad Sci USA 89: 5951-5955.

Okada, Y.C. 1997. Genesis of MEG signals in a mammalian CNS structure. Electroencephalogr Clin Neurophysiol 103, 474-485.

Parkes, L.M. 2007. Inability to Directly Detect Magnetic Field Changes Associated With Neuronal Activity. Magn Reson Med 57: 411-416.

Pell, G.S. 2006. Further steps toward direct magnetic resonance (MR) imaging detection of neural action currents: Optimization of MR sensitivity to transient and weak currents in a conductor. Magn Reson Med 55: 1038-1046.

Petridou, N. 2006. Direct magnetic resonance detection of neuronal electrical activity. Proc Natl Acad Sci USA 103: 16015-16020.

Romani, G.L. 1989. Fundamentals on neuromagnetism. In: Advances in biomagnetics, edited by S. Wiliamson. New York: Plenum Press.

Schulz, M. 2004. An integrative MEG-fMRI study of the primary somatosensory cortex using cross-modal correspondence analysis. NeuroImage 22: 120-133.

Schumann, C.M. 2005. Stereological estimation of the number of neurons in the human amygdaloid complex. J Comp Neurol 491: 320-329.

Scott, G.C, 1992. RF current density imaging in homogeneous media. Magn Reson Med 28: 186-201.

Singh, M. 1994. Sensitivity of MR phase shift to detect evoked neuromagnetic fields inside the head. IEEE Trans Nucl Sci 41: 349-351.

Song, A.W. 2001. Lorentz effect imaging. Magn Reson Imaging 19: 763-767.

Swinney, K.R. 1980. A calculation of the magnetic field of a nerve action potential. Biophys J 32: 719-731.

Tang, L. 2008. Failure to direct detect magnetic field dephasing corresponding to ERP generation. Magn Reson Imaging. 26:484-489

Truong, T.K. 2006. Finding neuroelectric activity under magnetic-field oscillations (NAMO) with magnetic resonance imaging in vivo. Proc Natl Acad Sci USA 103: 12598-12601.

Weaver, C.M. 2004. Automated algorithms for multiscale morphometry of neuronal dendrites. Neural Comput 16, 1353-1383.

Weisskoff, R.M. 1994. Microscopic susceptibility variation and transverse relaxation:

theory and experiment. Magn Reson Med 31, 601-610.

Wikswo, J.P. 1989. Biomagnetic sources and their models. In: Advances in biomagnetics, edited by S. Wiliamson. New York: Plenum Press.

Williams, S.R. 2002. Dependence of EPSP efficacy on synapse location in neocortical pyramidal neurons. Science 295: 1907-1910.

Xiong, J. 2003a. Directly mapping magnetic field effects of neuronal activity by magnetic resonance imaging. Human Brain Mapp 20, 41-49.

Xiong, J. 2003b. Estimation of effects of neuronal magnetic fields on MRI signals. Proc Of ISMRM.

Xue, Y. 2006. Direct MRI detection of neuronal magnetic fields in the brain: theoretical modeling. Neuroimage 31: 550-559.